Skyrmion-induced anomalous Hall conductivity on topological insulator surfaces

Yasufumi Araki[1,2] and Kentaro Nomura[1]

[1]*Institute for Materials Research, Tohoku University, Sendai 980-8577, Japan*
[2]*Frontier Research Institute for Interdisciplinary Sciences, Tohoku University, Sendai 980-8578, Japan*

Electron spin-momentum locking together with background magnetic textures can significantly alter the electron transport properties. We theoretically investigate the electron transport at the interface between a topological insulator and a magnetic insulator with magnetic skyrmions on the top. In contrast to the conventional topological Hall effect in normal metals, the skyrmions yield an additional contribution to the anomalous Hall conductivity even in the absence of in-plane magnetic texture, arising from the phase factor characteristic to Dirac electrons acquired at skyrmion boundary.

PACS numbers: 12.39.Dc, 75.70.-i, 73.43.-f, 71.70.Ej

arXiv:1704.05689v1 [cond-mat.mes-hall] 19 Apr 2017

Introduction — Physics of magnetic textures has been a significant topic in recent studies on magnetic materials, to make use of them as efficient carriers of information [1–3]. Skyrmion, in particular, is a particlelike magnetic excitation with a swirling texture in two dimensions (2D), in which the spin at the core and those at the perimeter point in the opposite directions [4, 5]. Such non-collinear magnetic textures are observed in non-centrosymmetric magnets, such as helimagnetic conductor MnSi (Refs. 6, 7) and magnetic insulator (MI) Cu_2OSeO_3 (Refs. 8, 9). The skyrmions form a periodic lattice, called skyrmion crystal, with the lattice constant around 10-100nm. One of the most important issues characteristic to skyrmions is the idea of emergent magnetic field for conduction electrons, arising from nonzero Berry curvature in the real space [10, 11]. A conduction electron propagating across the magnetic texture feels the emergent magnetic field, leading to the so-called topological Hall effect (THE) [12–15]. The topological Hall conductivity is determined by the skyrmion density, and is independent of the details of the skyrmions, such as the size or the texture.

In the presence of strong spin-orbit coupling (SOC), on the other hand, the band topology in the momentum space significantly affects the electron transport as well [16]. A typical example is the surface state of a topological insulator (TI), where the electrons show 2D linear dispersion with a single band-touching (Dirac) point [17, 18]. Under a finite out-of-plane magnetization, the Dirac point is gapped out and the system acquires a finite Chern number $C = \pm 1$ from the momentum-space Berry curvature, leading to the well-known quantum anomalous Hall effect (quantum AHE, QAHE) [19–24]. Since the exchange coupling between the local in-plane magnetization and the TI surface electron can be regarded as the emergent gauge field (vector potential) for the conduction electrons [25], topological magnetic textures on TI surfaces can give rise to even richer electronic properties: vortices and domain walls, for instance, are supposed to host zero modes, leading to electric charging of those textures [26–28]. Recent theoretical studies predict that magnetic skyrmions on TI surface can be charged as well [29, 30]. Transport measurements in magnetic TI heterostructures discovered the coexistence of the THE related to the real-space Berry curvature from skyrmions and the AHE related to momentum-space counterpart from SOC [31], while the transport is dominated by the bulk states, leaving the surface transport ambiguous.

In this work, we theoretically examine the electron transport on TI surface in the presence of skyrmions, which possibly accounts for the interface between a TI and a non-centrosymmetric MI. We fully solve the electron scattering problem by a single skyrmion, and apply its result to the Boltzmann transport theory to estimate the longitudinal and Hall conductivities. The skyrmions give a sizable additive contribution to the AHE, due to the skewness in the electron scattering at a skyrmion. The origin of this skewness is the phase factor acquired at the skyrmion boundary, which is characteristic to Dirac electrons and is absent in Schrödinger electron systems. It does not require the in-plane magnetization components, which is totally different from the well-known THE in normal metals. In this paper, we take $\hbar = 1$ and restore it in the final numerical results.

Electron scattering by a single skyrmion. — We first place a single skyrmion at the center of the 2D infinite space, to examine how an incoming electron plane wave gets scattered by the skyrmion. The electron on TI surface under the magnetic texture $\boldsymbol{n}(\boldsymbol{r})$ is described by the Hamiltonian

$$\mathcal{H} = v_{\rm F}(\hat{\boldsymbol{p}} \times \boldsymbol{\sigma})_z - \Delta \boldsymbol{n}(\boldsymbol{r}) \cdot \boldsymbol{\sigma}, \tag{1}$$

where the coefficient $v_{\rm F}$ is the Fermi velocity, $\hat{\boldsymbol{p}} = -i\boldsymbol{\nabla}$ is the momentum operator, and Δ is the spin splitting energy from the exchange interaction between the electron and the magnetization. The local in-plane magnetization texture $\boldsymbol{n}_{\parallel}(\boldsymbol{r})$ serves as the "emergent" gauge field $\boldsymbol{a} = (\Delta/v_{\rm F})\boldsymbol{e}_z \times \boldsymbol{n}_{\parallel}$ for the electrons, leading to the emergent magnetic field $b_z = (\boldsymbol{\nabla} \times \boldsymbol{a})_z = (\Delta/v_{\rm F})\boldsymbol{\nabla} \cdot \boldsymbol{n}_{\parallel}$ (Refs. 25, 26). In the numerical results below, we fix the parameters $v_{\rm F} = 0.5 \times 10^6$ m/s and $\Delta = 10$ meV,

which are typical values in TI-MI heterostructures, such as Bi_2Se_3 and yttrium iron garnet (YIG) [32, 33].

We here fix the skyrmion texture unaffected by the interface electrons, assuming that it is stabilized by the non-collinear spin correlation in the MI, such as the Dzyaloshinskii-Moriya interaction (DMI). It can be parametrized by the polar coordinate $\boldsymbol{r} = (\rho, \phi)$ as

$$n_z = n_z(\rho),\ \boldsymbol{n}_\parallel = \sqrt{1-n_z^2(\rho)} \begin{pmatrix} \cos(\phi+\Omega) \\ \sin(\phi+\Omega) \end{pmatrix}, \quad (2)$$

where $n_z(\rho)$ is a scalar function taking the value between -1 at the center and $+1$ at the perimeter. The angle Ω characterizes the internal texture of the skyrmion: $\Omega = 0$ (π) corresponds to a hedgehog skyrmion with the magnetization pointing outward (inward), while $\Omega = \pi/2$ ($3\pi/2$) to a vortex skyrmion with counterclockwise (clockwise) vorticity. Here we take a vortex skyrmion with $\Omega = \pi/2$, which is energetically more stable than a hedgehog skyrmion under the DMI [4, 5]. Since the eigenstate structure is qualitatively insensitive to the boundary thickness due to the absence of the emergent magnetic field b_z, we employ the "hard-wall" approximation $n_z(\rho) = \mathrm{sgn}(\rho - R_\mathrm{S})$, with R_S the skyrmion radius [29]. Such a structure is likely to be realized under a strong out-of-plane magnetic anisotropy. It does not induce the THE in normal metals due to the absence of the real-space Berry curvature, while it still poses nontrivial effects to Dirac electrons.

It is inadequate to treat the skyrmion texture on the TI surface perturbatively, since it fails to incorporate the topological characteristics, namely the change in the Chern number inside the skyrmion. We therefore need to solve the scattering problem of a Dirac electron by a single skyrmion non-perturbatively [34, 35]. The scattering process is characterized by the "phase shifts" of the eigenstates, which are the angles quantifying how much the eigenstates are altered by the skyrmion [36].

Since the Hamiltonian is invariant under the simultaneous rotation in the real and spin spaces around the z-axis, the total angular momentum $j = \pm 1/2, \pm 3/2, \cdots \in \mathbb{Z} + 1/2$ serves as a good quantum number. The eigenstate wave function with the angular momentum j can be parametrized as $\psi_j(\boldsymbol{r}) = [u_j(\rho)e^{i(j-\frac{1}{2})\phi}, v_j(\rho)e^{i(j+\frac{1}{2})\phi}]^T$. The radial equations for $u_j(\rho)$ and $v_j(\rho)$ can be analytically solved under the hard-wall approximation (see the Supplemental Material for detail). The radial solution behaves as a cylindrical wave, with the asymptotic wave number $k_\mathrm{F} = v_\mathrm{F}^{-1}\sqrt{E_\mathrm{F}^2 - \Delta^2}$ away from the skyrmion center ($\rho \to \infty$), for the conduction electron at the Fermi level $E_\mathrm{F} (> \Delta)$. The phase shift of this cylindrical wave relative to the skyrmion-free solution is determined by the boundary condition at the skyrmion edge R_S, as

$$\tan\delta_j = \frac{-2\Delta}{(E_\mathrm{F}+\Delta)T_{j+\frac{1}{2}} - (E_\mathrm{F}-\Delta)T_{j-\frac{1}{2}}}, \quad (3)$$

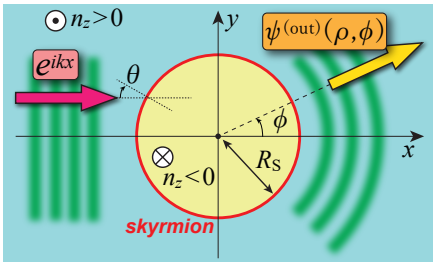

FIG. 1: Schematic picture of the electron scattering by a single skyrmion. An incident plane wave is scattered by a single skyrmion placed at the center, leaving the outgoing spherical wave $\psi^{(\mathrm{out})}(\rho, \phi)$. θ denotes the incident angle to the skyrmion boundary.

for each angular momentum mode j. Here $T_l \equiv Y_l(k_\mathrm{F}R_\mathrm{S})/J_l(k_\mathrm{F}R_\mathrm{S})$, with J_l the Bessel function and Y_l the Neumann function. With this phase shift δ_j, the asymptotic behavior of the partial wave away from the skyrmion can be expressed as

$$\psi_{k_\mathrm{F},j}(\rho,\phi) \sim \frac{1}{\sqrt{\rho}} \begin{pmatrix} \sin\frac{\zeta}{2}\cos(\xi_j + \frac{\pi}{4} - \delta_j)e^{i(j-\frac{1}{2})\phi} \\ -\cos\frac{\zeta}{2}\sin(\xi_j + \frac{\pi}{4} - \delta_j)e^{i(j+\frac{1}{2})\phi} \end{pmatrix}, \quad (4)$$

where $\xi_j \equiv k_\mathrm{F}\rho - \frac{\pi}{2}(j+\frac{1}{2})$ and $\cos\zeta \equiv \Delta/E_\mathrm{F}$. Negative δ_j implies the "repulsive" scattering process, while positive δ_j to the "attractive" scattering, for each partial wave component j.

If a plane wave with the incident wave vector $\boldsymbol{k} = (k_\mathrm{F}, 0)$ is scattered by the skyrmion placed at the origin, as shown in Fig. 1(a), we can set up an ansatz for the total wave function away from the skyrmion ($\rho \to \infty$) as

$$\Psi(\boldsymbol{r}) \sim e^{ik_\mathrm{F}x} \begin{pmatrix} -i\sin\frac{\zeta}{2} \\ \cos\frac{\zeta}{2} \end{pmatrix} + \frac{e^{ik_\mathrm{F}\rho}}{\sqrt{\rho}} \begin{pmatrix} f_\uparrow(\phi) \\ f_\downarrow(\phi) \end{pmatrix}, \quad (5)$$

where the first term comes from the incoming plane wave in the x-direction, while the second term corresponds to the outgoing scattered waves, which we denote $\psi^{(\mathrm{out})}(\rho, \phi)$ here. Since the total wave function on the right hand side can be given as a linear combination of the eigenfunctions $\{\psi_{k_\mathrm{F},j}\}$, we can estimate the scattering amplitudes $f_{\uparrow/\downarrow}(\phi)$ by the partial wave decomposition: by decomposing both sides of Eq. (5) and comparing the radial parts for each partial wave component, we obtain the scattering amplitudes

$$\begin{pmatrix} f_\uparrow(\phi) \\ f_\downarrow(\phi) \end{pmatrix} = \frac{1}{\sqrt{2\pi k_\mathrm{F}}} e^{i\frac{\pi}{4}} \Phi(\phi) \begin{pmatrix} \sin\frac{\zeta}{2}e^{-i\phi/2} \\ -\cos\frac{\zeta}{2}e^{i\phi/2} \end{pmatrix}, \quad (6)$$

where the angular function $\Phi(\phi)$ is composed of the phase shifts as

$$\Phi(\phi) = \sum_{j\in\mathbb{Z}+1/2} e^{ij\phi}(1 - e^{-2i\delta_j}). \quad (7)$$

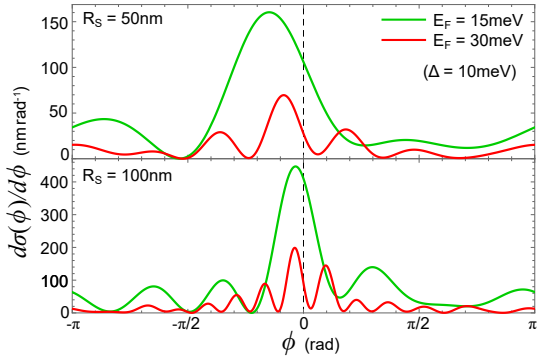

FIG. 2: The angular profile of the differential cross section $d\sigma(\phi)/d\phi$ induced by a hard-wall skyrmion, with its radius $R_{\rm S} = 50$nm in the upper panel and $R_{\rm S} = 100$nm in the lower panel.

Here it should be noted that the contribution from sufficiently large j, namely $|j| \gg k_{\rm F}R_{\rm S}$, is negligible in this summation, since the phase shift approaches zero with the asymptotic behavior $\delta_j \sim O[(k_{\rm F}R_{\rm S}/2\tilde{j})^{2\tilde{j}}]$ ($\tilde{j} \equiv |j|+1/2$) in this regime (see the Supplemental Material). It can be well understood in the semiclassical picture: if the impact parameter $|y| = |j|/k_{\rm F}$, namely the distance from the scattering center to the incident trajectory, is much larger than the skyrmion radius $R_{\rm S}$, the incident particle is almost unaffected by the skyrmion. Thus, we shall limit the partial waves to $|j| < 2k_{\rm F}R_{\rm S}+1$ in the calculations below.

Using the outgoing wave function $\psi^{(\rm out)}$ obtained above, the differential cross section, namely the ratio between the incoming current density $j^{(\rm in)}$ and the outgoing flux $j^{(\rm out)}(\phi)\rho d\phi$ toward the angle ϕ, is given by

$$\frac{d\sigma(\phi)}{d\phi} = \frac{j^{(\rm out)}\rho}{j^{(\rm in)}} = \frac{2E_{\rm F}}{v_{\rm F}k_{\rm F}}{\rm Im}\left[e^{-i\phi}f_\uparrow^* f_\downarrow\right] = \frac{|\Phi(\phi)|^2}{2\pi k_{\rm F}}. \quad (8)$$

The angular profile of the differential cross section $d\sigma(\phi)/d\phi$ is shown in Fig. 2, for several Fermi energies $E_{\rm F}$ and skyrmion radii $R_{\rm S}$. In contrast to normal scattering processes, such as the scattering of Schrödinger electrons by a symmetric Coulomb potential, the scattering process shows a skewness, asymmetric about $\phi = 0$.

The scattering skewness shown here can be traced back to the geometric phase acquired at the skyrmion boundary, which is characteristic to Dirac electrons. When an electron is transmitted through the boundary between two regions with opposite magnetizations, the scattered wave acquires a phase factor $e^{i\gamma(\theta)}$ relative to the incident wave, depending on its incident angle θ. In the electron scattering process treated here, the incident angle θ at the skyrmion boundary depends on the impact parameter y, at sufficiently long wavelength such that the uncertainty in y can be neglected (see Fig. 1). Therefore, the phase factor $e^{i\gamma(\theta)}$ depends on y; since this phase can be expanded as $\gamma(\theta(y)) = \pi + \tilde{k}y + O(y^2)$ around the scattering center, the linear part $e^{i\tilde{k}y}$ gives rise to the transverse wave, leading to the scattering skewness (see the Supplemental Material for detail).

Skyrmion-induced modulation of conductivity. — The electron scattering by skyrmions alters the electronic transport properties, the longitudinal and Hall conductivities in particular. Here we set up a uniformly magnetized 2D system with an ensemble of skyrmions, with the number density $n_{\rm S}$. If the skyrmion distribution is random and dilute enough, averaging over scattering paths within the finite range inside the skyrmions rules out quantum interference from multiple scattering processes, which enables us to employ the semiclassical Boltzmann theory. The electron transport under an electric field $\boldsymbol{E} = E_x\boldsymbol{e}_x$ is described by the Boltzmann equation,

$$\dot{\boldsymbol{k}}\cdot\nabla_{\boldsymbol{k}}f(\boldsymbol{k}) = [df(\boldsymbol{k})/dt]_{\rm coll}\,, \quad (9)$$

for the steady-state electron distribution $f(\boldsymbol{k})$. The coherent motion of a single wave packet is approximately described by the classical equations of motion, $\dot{\boldsymbol{r}} = \boldsymbol{v}(\boldsymbol{k}) - \dot{\boldsymbol{k}}\times\boldsymbol{\Omega}_{\boldsymbol{k}}$ and $\dot{\boldsymbol{k}} = -e\boldsymbol{E}$, where $\boldsymbol{v}(\boldsymbol{k}) = \boldsymbol{\nabla}_{\boldsymbol{k}}E(\boldsymbol{k})$ is the group velocity, and $\boldsymbol{\Omega}_{\boldsymbol{k}} = i(\nabla_{\boldsymbol{k}}\psi_{\boldsymbol{k}}^\dagger)\times(\nabla_{\boldsymbol{k}}\psi_{\boldsymbol{k}})$ is the momentum-space Berry curvature. The scattering process is incorporated in the collision term

$$\left(\frac{df(\boldsymbol{k})}{dt}\right)_{\rm coll} = -\frac{1}{\tau_0}\left[f(\boldsymbol{k}) - f_0(\boldsymbol{k})\right] - n_{\rm S}\int d\phi\; v(\boldsymbol{k})\left[\frac{d\sigma(\phi)}{d\phi}f(\boldsymbol{k}) - \frac{d\sigma(-\phi)}{d\phi}f(\boldsymbol{k}')\right]. \quad (10)$$

The second term describes the skyrmion-induced scattering process from momentum $\boldsymbol{k}$ into $\boldsymbol{k}'$ and vice versa, with ϕ the angle between them, while we introduce the effect of normal impurities by the first term phenomenologically in terms of relaxation-time approximation, with the transport relaxation time τ_0 and the equilibrium distribution $f_0(\boldsymbol{k})$. The momenta $\boldsymbol{k}$ and $\boldsymbol{k}'$ are limited to the Fermi surface, i.e. $|\boldsymbol{k}| = |\boldsymbol{k}'| = k_{\rm F}$, due to the elasticity of the scattering process. The asymmetry in the scattering amplitude, $d\sigma(\phi)/d\phi \neq d\sigma(-\phi)/d\phi$, violates the reciprocity between the process from $\boldsymbol{k}'$ to $\boldsymbol{k}$ and its inverse process, which may lead to the anomalous Hall transport. Here we focus on the leading-order effect in scattering, parametrized by τ_0^{-1} and $n_{\rm S}$, which rules out the velocity renormalization effect from the side-jump process [37].

The steady-state distribution $f(\boldsymbol{k})$ can be obtained up to the linear response in the electric field $\boldsymbol{E}$. Taking the ansatz [35]

$$\delta f(\boldsymbol{k}) = \left.\frac{\partial f_0}{\partial E}\right|_{E(\boldsymbol{k})}\left[(\boldsymbol{k}\cdot e\boldsymbol{E})C_k + (\boldsymbol{e}_z\times\boldsymbol{k}\cdot e\boldsymbol{E})D_k\right] \quad (11)$$

for the deviation of the distribution function $\delta f(\boldsymbol{k}) = f(\boldsymbol{k}) - f_0(\boldsymbol{k})$, we can straightforwardly solve the Botlz-

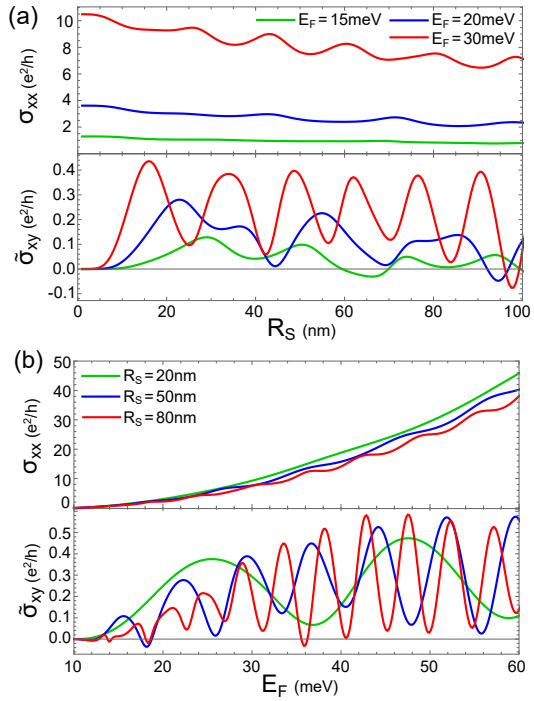

FIG. 3: The behavior of the skyrmion-modulated longitudinal conductivity, σ_{xx}, and the skyrmion contribution to the Hall conductivity, $\tilde{\sigma}_{xy}$, (a) with the Fermi energy $E_{\rm F}$ fixed and the skyrmion radius $R_{\rm S}$ varied, and (b) with $R_{\rm S}$ fixed and $E_{\rm F}$ varied, under the magnetic exchange energy $\Delta = 10$meV.

mann equation at zero temperature, yielding

$$\begin{pmatrix} C_k \\ D_k \end{pmatrix} = \frac{1}{(n_{\rm S}F_\parallel + \frac{E_{\rm F}}{v_{\rm F}\tau_0})^2 + (n_{\rm S}F_\perp)^2} \begin{pmatrix} n_{\rm S}F_\parallel + \frac{E_{\rm F}}{v_{\rm F}\tau_0} \\ n_{\rm S}F_\perp \end{pmatrix}. \tag{12}$$

Here $F_\parallel$ and $F_\perp$ characterize the amplitudes of backscattering and skew scattering at a skyrmion, respectively, defined by

$$\begin{pmatrix} F_\parallel \\ F_\perp \end{pmatrix} = \int \frac{d\phi}{2\pi} |\Phi(\phi)|^2 \begin{pmatrix} 1-\cos\phi \\ \sin\phi \end{pmatrix} = \sum_j \begin{pmatrix} 2\sin^2\bar{\delta}_j \\ \sin 2\bar{\delta}_j \end{pmatrix}, \tag{13}$$

with $\bar{\delta}_j = \delta_{j+1} - \delta_j$.

Once we obtain the distribution shift $\delta f(\boldsymbol{k})$ driven by the electric field, we can estimate its contribution to the current by $\tilde{\boldsymbol{j}} = -(e/V)\sum_{\boldsymbol{k}} \boldsymbol{v}(\boldsymbol{k})\delta f(\boldsymbol{k})$, leading to the conductivity coefficients

$$\tilde{\sigma}_{xx} = \frac{e^2}{4\pi}k_{\rm F}^2 C_k, \quad \tilde{\sigma}_{xy} = -\frac{e^2}{4\pi}k_{\rm F}^2 D_k. \tag{14}$$

The longitudinal part $\tilde{\sigma}_{xx}$ comes from the backscattering effect by the normal scatterers and the skyrmions, which is the dominant contribution to the longitudinal conductivity. Hence, we identify $\tilde{\sigma}_{xx}$ as the total longitudinal conductivity σ_{xx} here. On the other hand, it should be noted that $\tilde{\sigma}_{xy}$ obtained here is the additive contribution to the Hall conductivity induced by the skyrmions; we originally have the ordinary Hall effect contribution from the external magnetic field, the intrinsic contribution from the momentum-space Berry curvature [19], and the extrinsic contribution from the normal scatterers [37–41] as well, which are neglected in our Boltzmann analysis.

Now we focus on the behavior of skyrmion-modulated conductivities $(\sigma_{xx}, \tilde{\sigma}_{xy})$ as functions of Fermi energy $E_{\rm F}$ and the skyrmion radius $R_{\rm S}$, which are shown in Fig. 3. We take screened Coulomb impurities as the normal scatterers, which give the transport relaxation time τ_0 proportional to $n_{\rm c}^{-1/2}$, with $n_{\rm c} = k_{\rm F}^2/4\pi$ the carrier density [42–45]. Here we employ the calculation result in Ref. 45 obtained for graphene deposited on SiO_2 substrate, yielding $\tau_0 = 0.6{\rm ps} \times (k_{\rm F}/0.1{\rm nm}^{-1})$ under the impurity density $n_{\rm i} = 10^{11}{\rm cm}^{-2}$. The skyrmion number density $n_{\rm S}$ is fixed to $2.89 \times 10^9{\rm cm}^{-2}$, corresponding to the triangular skyrmion lattice with the spacing 200nm. It can be seen that the contribution to the Hall conductivity is suppressed at small $E_{\rm F}$ around the band bottom, due to the loss of spin-momentum locking and the enhancement of the normal scattering rate τ_0^{-1}.

From the results of Ref. 37, we can make an order estimation of the normal impurity contribution to the Hall conductivity, which is beyond the scope of our Boltzmann analysis. If the impurity distribution is Gaussian, its effect on the Hall conductivity is insensitive to the impurity potential strength and scales by $\lesssim (e^2/4\pi)(\Delta/E_{\rm F})$ for $E_{\rm F} \gg \Delta$. If the distribution is beyond Gaussian, it acquires an additional term from the third-order moment of the impurity distribution, corresponding to the skew scattering effect by the impurities. It is known to be inversely proportional to the scattering strength, scaling as $\sim (e^2/4\pi)(\Delta/n_{\rm i}V_{\rm i})$, where $V_{\rm i}$ parametrizes the impurity potential in terms of delta-function potential. At high $E_{\rm F}$, the impurity potential $V_{\rm i}$ gets reduced by strong screening, leading to enhancement of this third-order moment contribution. For $E_{\rm F} \sim 50$meV and $n_{\rm i} \sim 10^{11}{\rm cm}^{-2}$, the denominator $n_{\rm i}V_{\rm i}$ is around 10meV, estimated from the screened Coulomb potential [45]. Therefore, the skyrmion contribution to the anomalous Hall conductivity is comparable or even superior to the normal impurity contribution at $E_{\rm F} \sim 50$meV, which is possibly captured in transport measurements.

We find oscillatory behavior in both the longitudinal and Hall conductivities, as we vary the skyrmion radius $R_{\rm S}$ or the Fermi energy $E_{\rm F}$. Such quantum oscillations stem from the resonance states formed inside the skyrmion. In a 1D massive Dirac system, for instance, the electron transmission rate through a quantum well with the sign-flipped mass term is maximized if a standing wave is formed inside the well, i.e. $k_{\rm F}L = n\pi$ $(n \in \mathbb{Z})$, with L the size of the well. Here in the case of skyrmion, the skyrmion diameter $2R_{\rm S}$ plays the role of L. Hence

the neighboring peaks under the variation of $E_{\rm F}$ or $R_{\rm S}$ satisfy $(k_{\rm F}R_{\rm S})_{n+1} - (k_{\rm F}R_{\rm S})_n = \pi/2$, which coincides the inter-peak distances in the longitudinal conductivity σ_{xx} at large $E_{\rm F}$ and $R_{\rm S}$.

Variation of the Fermi energy $E_{\rm F}$ (or the Fermi momentum $k_{\rm F}$) can be experimentally realized by tuning the gate voltage or the carrier doping. If one can observe the quantum oscillations in the conductivities in such experiments, the size of skyrmions can be estimated by using the resonance condition mentioned above. The skyrmion size can also be modulated by external magnetic fields, thus leading to field-induced quantum oscillations in the conductivities, which should be distinguished from other quantum oscillations such as the Shubnikov–de Haas oscillation.

Discussion. — In this paper, we have investigated the electronic transport properties on TI surfaces in the presence of magnetic skyrmions. We have demonstrated that the skyrmions give rise to the extrinsic AHE and the quantum oscillations in conductivities, originating from the interplay between the magnetic texture and the Dirac band structure.

It should be noted that, in realistic magnetic materials, an external magnetic field is essential to stabilize skyrmions. In Cu_2OSeO_3, for instance, a magnetic field of ~ 0.05T is required, which corresponds to the magnetic length $\sim$ 100nm. The skyrmion size should not exceed this scale; otherwise the Landau quantization inside the skyrmion takes place and the scattering property obtained in this paper is no longer reliable.

We have so far relied on the hard-wall approximation on the skyrmion texture. Such an approximation is justified under strong out-of-plane magnetic anisotropy, which stabilizes out-of-plane magnetization pattern. As long as the skyrmion texture is vortex-like, the modification of the boundary condition can shift the starting point of the quantum oscillation, while the periodicity of the quantum oscillation is unaffected, since the resonance state is still formed in the (relatively) flat region inside the skyrmion. On the other hand, our results do not apply to the hedgehog skyrmion, due to the emergent magnetic flux. Such type of skyrmion is expected to be induced by frustrated exchange interactions or four-spin exchange interactions [4], whose effect on the electron transport on TI surfaces remains an open question.

The authors acknowledge T. Chiba, C. Lee, Y. Ominato, and K. Sato for fruitful discussions. Y. A. is supported by JSPS KAKENHI Grant Number JP15H06023. K. N. is supported by JSPS KAKENHI Grant Numbers JP26400308 and JP15H05854.

[1] I. Žutić, J. Fabian, and S. Das Sarma, Rev. Mod. Phys. **76**, 323 (2004).
[2] A. Brataas, G. E. W. Bauer, and P. J. Kelly, Phys. Rep. **427**, 157 (2006).
[3] G. Tatara, H. Kohno, and J. Shibata, Phys. Rep. **468**, 213 (2008).
[4] N. Nagaosa and Y. Tokura, Nat. Nanotechnol. **8**, 899 (2013).
[5] A. Fert, V. Cros, and J. Sampaio, Nat. Nanotechnol. **8**, 152 (2013).
[6] S. Mühlbauer, B. Binz, F. Jonietz, C. Pfleiderer, A. Rosch, A. Neubauer, R. Georgii, and P. Böni, Science **323**, 915 (2009).
[7] A. Tonomura, X. Yu, K. Yanagisawa, T. Matsuda, Y. Onose, N. Kanazawa, H. S. Park, and Y. Tokura, Nano Lett. **12**, 1673 (2012).
[8] S. Seki, X. Z. Yu, S. Ishiwata, and Y. Tokura, Science **336**, 198 (2012).
[9] T. Adams, A. Chacon, M. Wagner, A. Bauer, G. Brandl, B. Pedersen, H. Berger, P. Lemmens, and C. Pfleiderer, Phys. Rev. Lett. **108**, 237204 (2012).
[10] N. Nagaosa and Y. Tokura, Phys. Scr. **T146** 014020 (2012).
[11] N. Nagaosa, X. Z. Yu, and Y. Tokura, Phil. Trans. R. Soc. A **370**, 5806 (2012).
[12] J. Ye, Y. B. Kim, A. J. Millis, B. I. Shraiman, P. Majumdar, and Z. Tešanović, Phys. Rev. Lett. **83**, 3737 (1999).
[13] G. Tatara and H. Kawamura, J. Phys. Soc. Jpn. **71**, 2613 (2002).
[14] M. Lee, W. Kang, Y. Onose, Y. Tokura, and N. P. Ong, Phys. Rev. Lett. **102**, 186601 (2009).
[15] A. Neubauer, C. Pfleiderer, B. Binz, A. Rosch, R. Ritz, P. G. Niklowitz, and P. Böni, Phys. Rev. Lett. **102**, 186602 (2009).
[16] D. J. Thouless, M. Kohmoto, M. P. Nightingale, and M. den Nijs, Phys. Rev. Lett. **49**, 405 (1982).
[17] M. Z. Hasan and C. L. Kane, Rev. Mod. Phys. **82**, 3045 (2010).
[18] X.-L. Qi and S.-C. Zhang, Rev. Mod. Phys. **83**, 1057 (2011).
[19] X.-L. Qi, Y.-S. Wu, and S.-C. Zhang, Phys. Rev. B **74**, 085308 (2006).
[20] X.-L. Qi, T. L. Hughes, and S.-C. Zhang, Phys. Rev. B **78**, 195424 (2008).
[21] R. Yu, W. Zhang, H.-J. Zhang, S.-C. Zhang, X. Dai, and Z. Fang, Science **329**, 61 (2010).
[22] K. Nomura and N. Nagaosa, Phys. Rev. Lett. **106**, 166802 (2011).
[23] J. G. Checkelsky, J. Ye, Y. Onose, Y. Iwasa, and Y. Tokura, Nat. Phys. **8**, 729 (2012).
[24] C.-Z. Chang, J. Zhang, X. Feng, J. Shen, Z. Zhang, M. Guo, K. Li, Y. Ou, P. Wei, L.-L. Wang, Z.-Q. Ji, Y. Feng, S. Ji, X. Chen, J. Jia, X. Dai, Z. Fang, S.-C. Zhang, K. He, Y. Wang, L. Lu, X.-C. Ma, and Q.-K. Xue, Science **340**, 167 (2013).
[25] I. Garate and M. Franz, Phys. Rev. Lett. **104**, 146802 (2010).
[26] K. Nomura and N. Nagaosa, Phys. Rev. B **82**, 161401 (2010).
[27] Y. Tserkovnyak and D. Loss, Phys. Rev. Lett. **108**, 187201 (2012).
[28] Y. Tserkovnyak, D. A. Pesin, and D. Loss, Phys. Rev. B **91**, 041121 (2015).
[29] H. M. Hurst, D. K. Efimkin, J. Zang, and V. Galitski, Phys. Rev. B **91**, 060401 (2015).
[30] D. Andrikopoulos, B. Soré, and J. De Boeck, J. Appl. Phys. **119**, 193903 (2016).
[31] K. Yasuda, R. Wakatsuki, T. Morimoto, R. Yoshimi,

A. Tsukazaki, K. S. Takahashi, M. Ezawa, M. Kawasaki, N. Nagaosa, and Y. Tokura, Nat. Phys. **12**, 555 (2016).
[32] W. Liu, L. He, Y. Zhou, K. Murata, M. C.Onbasli, C. A. Ross, Y. Jiang, Y. Wang, Y. Xu, R. Zhang, and K. L. Wang, AIP Advances **6**, 055813 (2016).
[33] Y. Kubota, K. Murata, J. Miyawaki, K. Ozawa, M. C. Onbasli, T. Shirasawa, B. Feng, Sh. Yamamoto, R.-Y. Liu, S. Yamamoto, S. K. Mahatha, P. Sheverdyaeva, P. Moras, C. A. Ross, S. Suga, Y. Harada, K. L. Wang, and I. Matsuda, J. Phys.: Condens. Matter **29** 055002 (2017).
[34] A. Ferreira, J. Viana-Gomes, J. Nilsson, E. R. Mucciolo, N. M. R. Peres, and A. H. Castro Neto, Phys. Rev. B **83**, 165402 (2011).
[35] A. Ferreira, T. G. Rappoport, M. A. Cazalilla, and A. H. Castro Neto, Phys. Rev. Lett. **112**, 066601 (2014).
[36] R. G. Newton, *Scattering Theory of Waves and Particles: Second Edition* (Springer-Verlag, New York, 1982).
[37] N. A. Sinitsyn, A. H. MacDonald, T. Jungwirth, V. K. Dugaev, and J. Sinova, Phys. Rev. B **75**, 045315 (2007).
[38] N. A. Sinitsyn, J. Phys.: Condens. Matter **20**, 023201 (2008).
[39] D. Culcer and S. Das Sarma, Phys. Rev. B **83**, 245441 (2011).
[40] H.-Z. Lu and S.-Q. Shen, Phys. Rev. B **88**, 081304 (2013).
[41] I. A. Ado, I. A. Dmitriev, P. M. Ostrovsky, and M. Titov, EPL **111**, 37004 (2015).
[42] K. Nomura and A. H. MacDonald, Phys. Rev. Lett. **96**, 256602 (2006).
[43] K. Nomura and A. H. MacDonald, Phys. Rev. Lett. **98**, 076602 (2007).
[44] T. Ando, J. Phys. Soc. Jpn. **75**, 074716 (2006).
[45] E. H. Hwang and S. Das Sarma, Phys. Rev. B **77**, 195412 (2008).

SUPPLEMENTAL MATERIAL

Eigenstate wave functions under a single skyrmion

In this part, we show the detailed derivation of the eigenstate wave functions under a single skyrmion, which leads to the phase shift [Eq. (3)]. For the partial wave component with the total angular momentum $j(=\pm 1/2, \pm 3/2, \cdots)$, we can set up the ansatz

$$\psi_j(\rho,\phi) = \begin{pmatrix} u_j(\rho)e^{il_\uparrow\phi} \\ v_j(\rho)e^{il_\downarrow\phi} \end{pmatrix}, \tag{15}$$

with $l_{\uparrow/\downarrow} \equiv j \mp 1/2$ the orbital angular momentum for each component. With this ansatz, the Dirac equation $\mathcal{H}\psi = E\psi$ reduces to the radial differential equation,

$$\begin{pmatrix} -\Delta n_z(\rho) - E & v_{\rm F}(-\partial_\rho - l_\downarrow\rho^{-1}) \\ v_{\rm F}(\partial_\rho - l_\downarrow\rho^{-1}) & \Delta n_z(\rho) - E \end{pmatrix} \begin{pmatrix} u_j(\rho) \\ v_j(\rho) \end{pmatrix} = 0, \tag{16}$$

under the hard-wall approximation on the skyrmion texture.

Let us solve the equation without skyrmion, namely with $n_z(\rho) = 1$ in the entire system, as the starting point. Here the equation reads

$$\begin{pmatrix} -\Delta - E & v_{\rm F}(-\partial_\rho - l_\downarrow\rho^{-1}) \\ v_{\rm F}(\partial_\rho - l_\downarrow\rho^{-1}) & \Delta - E \end{pmatrix} \begin{pmatrix} u_j(\rho) \\ v_j(\rho) \end{pmatrix} = 0. \tag{17}$$

Using the relation

$$v_j(\rho) = -\frac{v_{\rm F}}{\Delta - E}\left(\partial_\rho - \frac{l_\uparrow}{\rho}\right) u_j(\rho), \tag{18}$$

we obtain the second-order differential equation for u,

$$\left[\partial_\rho^2 + \frac{1}{\rho}\partial_\rho + \frac{E^2 - \Delta^2}{v_{\rm F}^2} - \frac{l_\uparrow^2}{\rho^2}\right] u_j(\rho) = 0. \tag{19}$$

With the radial wavenumber $k \equiv v_{\rm F}^{-1}\sqrt{E^2 - \Delta^2}$ and the change of variable $\xi \equiv k\rho$, Eq. (19) reduces to the well-known Bessel's differential equation,

$$\left[\partial_\xi^2 - \frac{1}{\xi}\partial_\xi + 1 - \frac{l_\uparrow^2}{\xi^2}\right] u_j(\xi) = 0, \tag{20}$$

whose linearly independent solutions are given by the Bessel function $J_{l_\uparrow}(\xi)$ and the Neumann function $Y_{l_\uparrow}(\xi)$. Since $Y_{l_\uparrow}$ is ruled out for solution due to the singularity at $\rho = 0$, we can set $u_j(\rho) = C_{k,j}^{(+)} J_{l_\uparrow}(k\rho)$ with C the normalization constant. Substituting this solution to Eq. (18), we obtain the eigenstate wave function

$$\chi_{k,j}^{(+)}(\rho,\phi) = C_{k,j}^{(+)} \begin{pmatrix} J_{l_\uparrow}(k\rho)e^{il_\uparrow\phi} \\ -\frac{v_{\rm F}k}{E-\Delta} J_{l_\downarrow}(k\rho)e^{il_\downarrow\phi} \end{pmatrix}, \tag{21}$$

where we have used the recurrence relation

$$\left(\partial_\xi \mp \frac{l}{\xi}\right) J_l(\xi) = \mp J_{l\pm1}(\xi). \tag{22}$$

The normalization condition

$$\int_0^\infty d\rho\ \rho \int_0^{2\pi} d\phi \left[\chi^{(+)}_{k,j}(\boldsymbol{r})\right]^\dagger \chi^{(+)}_{k',j}(\boldsymbol{r}) = \delta(k-k') \tag{23}$$

fixes the normalization constant as

$$2\pi \left|C^{(+)}_{k,j}\right|^2 \frac{1}{k}\left[1+\left(\frac{v_{\rm F}k}{E-\Delta}\right)^2\right] = 1, \tag{24}$$

where we have used the orthogonality relation

$$\int_0^\infty d\rho\ \rho J_l(k\rho)J_l(k'\rho) = \frac{1}{k}\delta(k-k'). \tag{25}$$

Therefore, the normalized eigenstate wave function is given by

$$\chi^{(+)}_{k,j}(\rho,\phi) = \sqrt{\frac{k}{2\pi}} \begin{pmatrix} \sin\frac{\zeta}{2} J_{l_\uparrow}(k\rho)e^{il_\uparrow\phi} \\ -\cos\frac{\zeta}{2} J_{l_\downarrow}(k\rho)e^{il_\downarrow\phi} \end{pmatrix}. \tag{26}$$

Here the angle ζ is defined by $E = \Delta/\cos\zeta$, so that it should satisfy

$$\frac{v_{\rm F}k}{E-\Delta} = \frac{\tan\zeta}{\sec\zeta - 1} = \frac{\sin\zeta}{1-\cos\zeta} = \cot\frac{\zeta}{2}. \tag{27}$$

We should note here the relation

$$J_{-l}(\xi) = (-1)^l J_l(\xi) \tag{28}$$

for integer l. If the magnetization is flipped, i.e. $n_z(\rho) = -1$, we should substitute ζ by $\pi-\zeta$, leading to the eigenfunction

$$\chi^{(-)}_{k,j}(\rho,\phi) = \sqrt{\frac{k}{2\pi}} \begin{pmatrix} \cos\frac{\zeta}{2} J_{l_\uparrow}(k\rho)e^{il_\uparrow\phi} \\ -\sin\frac{\zeta}{2} J_{l_\downarrow}(k\rho)e^{il_\downarrow\phi} \end{pmatrix}. \tag{29}$$

In the presence of a hard-wall skyrmion, i.e.

$$n_z(\rho < R_{\rm S}) = -1; \quad n_z(\rho > R_{\rm S}) = +1, \tag{30}$$

we should solve Eq. (17) inside and outside the skyrmion separately, and connect the solution at the boundary. Inside the skyrmion, the solution is given by Eq. (29). Outside the skyrmion, on the other hand, the solutions is not simply given by Eq. (26), since we do not need to respect the normalizability at the origin. The Neumann counterpart of $\chi^{(+)}_{k,j}$, given by

$$\eta^{(+)}_{k,j}(\rho,\phi) = \sqrt{\frac{k}{2\pi}} \begin{pmatrix} \sin\frac{\zeta}{2} Y_{l_\uparrow}(k\rho)e^{il_\uparrow\phi} \\ -\cos\frac{\zeta}{2} Y_{l_\downarrow}(k\rho)e^{il_\downarrow\phi} \end{pmatrix}, \tag{31}$$

also contributes to the solution. Thus the solution outside the skyrmion should be given by the linear combination,

$$\psi^{(+)}_{k,j}(\rho,\phi) = A_{k,j}\chi^{(+)}_{k,j}(\rho,\phi) + B_{k,j}\eta^{(+)}_{k,j}(\rho,\phi), \tag{32}$$

where the coefficients $A_{k,j}$ and $B_{k,j}$ are determined by the boundary condition

$$\chi^{(-)}_{k,j}(\rho\to R_{\rm S},\phi) = \psi^{(+)}_{k,j}(\rho\to R_{\rm S},\phi). \tag{33}$$

Thus we obtain the coupled equations for those coefficients,

$$\begin{pmatrix} J_{l_\uparrow}(kR_{\rm S}) & J_{l_\downarrow}(kR_{\rm S}) \\ Y_{l_\uparrow}(kR_{\rm S}) & Y_{l_\downarrow}(kR_{\rm S}) \end{pmatrix} \begin{pmatrix} A_{k,j} \\ B_{k,j} \end{pmatrix} = \begin{pmatrix} \cot\frac{\zeta}{2} J_{l_\uparrow}(kR_{\rm S}) \\ \tan\frac{\zeta}{2} J_{l_\downarrow}(kR_{\rm S}) \end{pmatrix}. \tag{34}$$

The equations can be exactly solved, yielding

$$\begin{pmatrix} A_{k,j} \\ B_{k,j} \end{pmatrix} = \frac{1}{T_{l_\downarrow} - T_{l_\uparrow}} \begin{pmatrix} \cot\frac{\zeta}{2} T_{l_\downarrow} - \tan\frac{\zeta}{2} T_{l_\uparrow} \\ \tan\frac{\zeta}{2} - \cot\frac{\zeta}{2} \end{pmatrix}, \tag{35}$$

with

$$T_l \equiv Y_l(kR_{\rm S})/J_l(kR_{\rm S}). \tag{36}$$

In order to meet the orthogonality relation

$$\int_0^\infty d\rho\ \rho \int_0^{2\pi} d\phi \left[\psi_{k,j}(\boldsymbol{r})\right]^\dagger \psi_{k',j}(\boldsymbol{r}) = \delta(k-k'), \tag{37}$$

the whole wave function $\psi_{k,j}(\boldsymbol{r})$ should be divided by the factor $C_{k,j} \equiv \sqrt{A^2_{k,j} + B^2_{k,j}}$, yielding the final solution

$$\psi_{k,j}(\rho,\phi) = \begin{cases} \frac{1}{C_{k,j}}\chi^{(-)}_{k,j}(\rho,\phi) & (\rho < R_{\rm S}) \\ \frac{A_{k,j}}{C_{k,j}}\chi^{(+)}_{k,j}(\rho,\phi) + \frac{B_{k,j}}{C_{k,j}}\eta^{(+)}_{k,j}(\rho,\phi) & (\rho > R_{\rm S}) \end{cases}. \tag{38}$$

The asymptotic behavior of this solution in the limit $\rho\to\infty$ is important in deriving the scattering amplitude. Using the asymptotic behavior of the Bessel functions for $\xi\to\infty$,

$$J_l(\xi) \sim \sqrt{\frac{2}{\pi\xi}}\left[\cos\left(\xi - \frac{l\pi}{2} - \frac{\pi}{4}\right) + O(\xi^{-1})\right] \tag{39}$$

$$Y_l(\xi) \sim \sqrt{\frac{2}{\pi\xi}}\left[\sin\left(\xi - \frac{l\pi}{2} - \frac{\pi}{4}\right) + O(\xi^{-1})\right], \tag{40}$$

their linear combination satisfies

$$\begin{aligned} &J_l(\xi)\cos\delta + Y_l(\xi)\sin\delta \\ &\sim \sqrt{\frac{2}{\pi\xi}}\left[\cos\left(\xi - \frac{l\pi}{2} - \frac{\pi}{4} - \delta\right) + O(\xi^{-1})\right], \end{aligned} \tag{41}$$

where δ serves as the phase shift of the cylindrical wave in comparison with the original wave J_l. Thus, by introducing the phase shift

$$\delta_j \equiv \arctan\frac{B_{k,j}}{A_{k,j}} \tag{42}$$

$$= -\arctan\frac{\cos^2\frac{\zeta}{2} - \sin^2\frac{\zeta}{2}}{\cos^2\frac{\zeta}{2}T_{l_\downarrow} - \sin^2\frac{\zeta}{2}T_{l_\uparrow}} \tag{43}$$

$$= -\arctan\frac{\cos\zeta}{\frac{1}{2}(1+\cos\zeta)T_{l_\downarrow} - \frac{1}{2}(1-\cos\zeta)T_{l_\uparrow}} \tag{44}$$

$$= -\arctan\frac{2\Delta}{(E+\Delta)T_{l_\downarrow} - (E-\Delta)T_{l_\uparrow}} \tag{45}$$

for each partial wave component, we obtain the asymptotic behavior

$$\psi_{k,j}(\rho\to\infty,\phi) \sim \sqrt{\frac{2}{\pi k\rho}}\begin{pmatrix} \sin\frac{\zeta}{2}\cos\left[k\rho-\frac{\pi}{2}l_\uparrow-\frac{\pi}{4}-\delta_j\right]e^{il_\downarrow\phi} \\ -\cos\frac{\zeta}{2}\cos\left[k\rho-\frac{\pi}{2}l_\downarrow-\frac{\pi}{4}-\delta_j\right]e^{il_\uparrow\phi}\end{pmatrix}. \tag{46}$$

For large angular momentum ($|j|\gg k_{\rm F}R_{\rm S}$), the asymptotic behavior of the phase shift is given by

$$\tan\delta_j = -\frac{2\Delta}{(E+\Delta)T_{l_\downarrow}-(E-\Delta)T_{l_\uparrow}} \tag{47}$$

$$\sim \frac{\Delta}{(E+\Delta)\left(\frac{2|l_\downarrow|}{ek_FR_{\rm S}}\right)^{2|l_\downarrow|}-(E-\Delta)\left(\frac{2|l_\uparrow|}{ek_FR_{\rm S}}\right)^{2|l_\uparrow|}} \tag{48}$$

$$\sim O\left[\left(\frac{k_{\rm F}R_{\rm S}}{2|j|+1}\right)^{2|j|+1}\right] \tag{49}$$

using the asymptotic behavior of the Bessel functions

$$J_l(\xi)\sim\frac{(\mathrm{sgn}l)^l}{|l|!}\left(\frac{\xi}{2}\right)^{|l|} \tag{50}$$

$$Y_l(\xi)\sim-\frac{(\mathrm{sgn}l)^l(|l|-1)!}{\pi}\left(\frac{\xi}{2}\right)^{-|l|} \tag{51}$$

$$\frac{Y_l(\xi)}{J_l(\xi)}\sim-\frac{(|l|!)^2}{\pi|l|}\left(\frac{2}{\xi}\right)^{2|l|}\sim-2\left(\frac{2|l|}{e\xi}\right)^{2|l|} \tag{52}$$

for $|l|\gg\xi$, with the Stirling's formula for the factorial (Gamma function)

$$n!=\Gamma(n+1)\overset{n\to\infty}{\sim}\sqrt{2\pi n}(n/e)^n. \tag{53}$$

Thus the phase shift for large angular momentum is suppressed, as mentioned in the main text.

The total wave function $\Psi(\boldsymbol{r})$ is given by the linear combination of the eigenstates obtained above, namely

$$\Psi(\boldsymbol{r})=\sum_{j\in\mathbb{Z}+1/2}\alpha_j\psi_{k,j}(\rho,\phi). \tag{54}$$

Derivation of scattering amplitude

Here we show the derivation process of the electron scattering amplitude by a single skyrmion, whose final result is given in Eq. (7). As mentioned in the main text, we consider here a case where an incident plane wave with the wave vector $\boldsymbol{k}$ and the energy $E=\sqrt{v_F^2|\boldsymbol{k}|^2+\Delta^2}$ is scattered by the skyrmion and comes out as a cylindrical wave with the wave number $k=|\boldsymbol{k}|$. The total wave function away from the skyrmion can be defined as the linear combination of the incident and outgoing waves,

$$\Psi(\boldsymbol{r})\sim\psi^{(\rm in)}_{\boldsymbol{k}}(\boldsymbol{r})+\psi^{(\rm out)}(\boldsymbol{r}), \tag{55}$$

with the incident plane wave

$$\psi^{(\rm in)}_{\boldsymbol{k}}(\boldsymbol{r})=e^{i\boldsymbol{k}\cdot\boldsymbol{r}}\begin{pmatrix}-i\sin\frac{\zeta}{2}\\ \cos\frac{\zeta}{2}\end{pmatrix}. \tag{56}$$

Here the outgoing wave component is defined by

$$\psi^{(\rm out)}(\boldsymbol{r})=\begin{pmatrix}f_\uparrow(\phi)\\ f_\downarrow(\phi)\end{pmatrix}\frac{e^{ik\rho}}{\sqrt{\rho}}, \tag{57}$$

with $f_{\uparrow/\downarrow}(\phi)$ the scattering amplitude for each spin component.

As in the scattering theory of Schrödinger electrons, the scattering amplitude can be calculated in terms of the partial-wave decomposition. Taking the x axis to the direction of the incident wave vector $\boldsymbol{k}$, the plane wave can be decomposed into partial waves as

$$\psi^{(\rm in)}_{\boldsymbol{k}}(\boldsymbol{r})=e^{ik\rho\cos\phi}\begin{pmatrix}-i\sin\frac{\zeta}{2}\\ \cos\frac{\zeta}{2}\end{pmatrix} \tag{58}$$

$$=\sum_{l\in\mathbb{Z}}i^lJ_l(k\rho)e^{il\phi}\begin{pmatrix}-i\sin\frac{\zeta}{2}\\ \cos\frac{\zeta}{2}\end{pmatrix}, \tag{59}$$

which shows the asymptotic behavior

$$\psi^{(\rm in)}_{\boldsymbol{k}}(\boldsymbol{r})\sim\sum_{l\in\mathbb{Z}}i^le^{il\phi}\sqrt{\frac{2}{\pi k\rho}}\cos\left(k\rho-\frac{l\pi}{2}-\frac{\pi}{4}\right)\begin{pmatrix}-i\sin\frac{\zeta}{2}\\ \cos\frac{\zeta}{2}\end{pmatrix}. \tag{60}$$

For the scattering amplitude, we define the partial-wave decomposition

$$f_\uparrow(\phi)\equiv\sum_{l_\uparrow\in\mathbb{Z}}\sqrt{\frac{2}{\pi k}}\sin\frac{\zeta}{2}\,g^\uparrow_{l_\uparrow}e^{il_\uparrow\phi} \tag{61}$$

$$f_\downarrow(\phi)\equiv\sum_{l_\downarrow\in\mathbb{Z}}\sqrt{\frac{2}{\pi k}}\cos\frac{\zeta}{2}\,g^\downarrow_{l_\downarrow}e^{il_\downarrow\phi}. \tag{62}$$

By comparing the both sides of Eq. (55) for each partial wave component in the limit $\rho\to\infty$, we obtain a sequence of equations

$$\alpha_j\cos\left[\xi_j-\delta_j\right]=-i^{l_\uparrow+1}\cos\xi_j+e^{i\xi}g^\uparrow_{l_\uparrow} \tag{63}$$

$$-\alpha_j\cos\left[\xi_j-\tfrac{\pi}{2}-\delta_j\right]=i^{l_\downarrow}\cos\left[\xi_j-\tfrac{\pi}{2}\right]+e^{i\xi}g^\downarrow_{l_\downarrow}, \tag{64}$$

where we use shorthand notations $\xi\equiv k\rho$, $\xi_j\equiv k\rho-(\pi/2)j$, and $l_{\uparrow/\downarrow}=j\mp1/2$. Since the second term in the right-hand side of each equation does not contribute to the incoming cylindrical wave $e^{-ik\rho}$, the incoming parts of Eqs. (63) and (64) give the same relation,

$$\alpha_je^{i[(\pi/2)j+\delta_j]}=-e^{i(\pi/2)(j+1/2)}e^{i(\pi/2)j}, \tag{65}$$

which fixes the value of the coefficient α_j as

$$\alpha_j=-e^{i[(\pi/2)(j+1/2)-\delta_j]}. \tag{66}$$

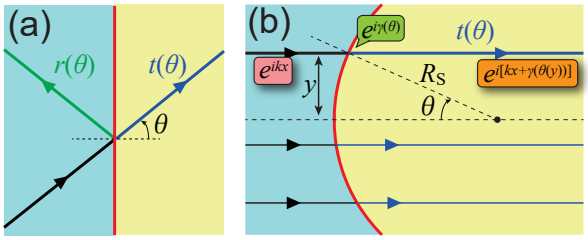

FIG. 4: Schematic pictures of the transmission of plane waves at the boundary between two regions with opposite magnetizations. (a) If a plane wave reaches a straight boundary, the complex transmission rate t and the reflection rate r depend on the incident angle θ. (b) If the boundary has a curvature, the incident angle θ depends on the lateral position y, leading to the position-dependent phase factor $e^{i\gamma(\theta(y))}$.

Substituting this relation to the outgoing ($e^{ik\rho}$) parts, we obtain

$$g^{\uparrow}_{l_\uparrow} = \frac{\alpha_j}{2} e^{-i[(\pi/2)j+\delta_j]} + \frac{1}{2} e^{i(\pi/2)(l_\uparrow+1)} e^{-i(\pi/2)j} \tag{67}$$

$$= \frac{1}{2} e^{i(\pi/4)} \left[1 - e^{-2i\delta_j}\right] \tag{68}$$

$$g^{\downarrow}_{l_\downarrow} = -\frac{\alpha_j}{2} e^{-i[(\pi/2)(j+1)+\delta_j]} - \frac{1}{2} e^{i(\pi/2)l_\downarrow} e^{-i(\pi/2)(j+1)} \tag{69}$$

$$= \frac{i}{2} e^{i(\pi/4)} \left[1 - e^{-2i\delta_j}\right]. \tag{70}$$

Thus the total scattering amplitude is given by

$$\begin{pmatrix} f_\uparrow(\phi) \\ f_\downarrow(\phi) \end{pmatrix} = \frac{1}{2} e^{i(\pi/4)} \sqrt{\frac{2}{\pi k}} \times \sum_{j\in\mathbb{Z}+1/2} \left(1 - e^{-2i\delta_j}\right) \begin{pmatrix} -i \sin\frac{\zeta}{2} e^{i(j-1/2)\phi} \\ \cos\frac{\zeta}{2} e^{i(j+1/2)\phi} \end{pmatrix}, \tag{71}$$

which further reduces to Eq. (6).

Phase factor on transmitted plane wave at skyrmion boundary

Here we give a detailed discussion on the geometric phase factor acquired at the skyrmion boundary, which leads to the scattering skewness, as briefly mentioned in the main text. We first start from the simplified geometry, where the region with $n_z = +1$ and that with $n_z = -1$ is separated by the straight boundary at $x = 0$, as shown in Fig. 4(a). If one takes a plane wave with the wave number k and the incident angle θ as the incident wave, its wave function is given by

$$\psi_{\rm i}(\boldsymbol{r}) = e^{ik(x\cos\theta + y\sin\theta)} \begin{pmatrix} -i\sin\frac{\zeta}{2} e^{-i\theta/2} \\ \cos\frac{\zeta}{2} e^{i\theta/2} \end{pmatrix}. \tag{72}$$

Due to the translational symmetry in y-direction, the y-component of the momentum is conserved through the transmission and reflection processes, yielding the transmitted and reflected wave functions

$$\psi_{\rm t}(\boldsymbol{r}) = e^{ik(x\cos\theta + y\sin\theta)} \begin{pmatrix} -i\cos\frac{\zeta}{2} e^{-i\theta/2} \\ \sin\frac{\zeta}{2} e^{i\theta/2} \end{pmatrix} \tag{73}$$

$$\psi_{\rm r}(\boldsymbol{r}) = e^{ik(-x\cos\theta + y\sin\theta)} \begin{pmatrix} -i\sin\frac{\zeta}{2} e^{-i(\pi-\theta)/2} \\ \cos\frac{\zeta}{2} e^{i(\pi-\theta)/2} \end{pmatrix}, \tag{74}$$

respectively. The complex transmission coefficient $t(\theta)$ and the reflection coefficient $r(\theta)$ should satisfy the boundary condition at $x = 0$,

$$\psi_{\rm i}(x=0;y) + r(\theta)\psi_{\rm r}(x=0;y) = t(\theta)\psi_{\rm t}(x=0;y). \tag{75}$$

Solving this equation, we obtain

$$t(\theta) = \frac{\cos\theta \sin\zeta}{\cos\theta - i\sin\theta\cos\zeta} \tag{76}$$

$$r(\theta) = \frac{i\cos\zeta}{\cos\theta - i\sin\theta\cos\zeta}. \tag{77}$$

One can easily check that these factors satisfy the conservation of flux,

$$|t(\theta)|^2 + |r(\theta)|^2 = 1. \tag{78}$$

The scattered wave, namely the deviation of the transmitted wave from the incident wave, is characterized by the factor

$$t(\theta) - 1 = \frac{\cos\theta(\sin\zeta - 1) + i\sin\theta\cos\zeta}{\cos\theta - i\sin\theta\cos\zeta} \tag{79}$$

$$= -(1-\sin\zeta)\frac{1 - i\cos\zeta(1-\sin\zeta)^{-1}\tan\theta}{1 - i\cos\zeta\tan\theta}, \tag{80}$$

which implies that the scattered wave acquires the geometric phase factor

$$e^{i\gamma(\theta)} = \frac{t(\theta)-1}{|t(\theta)-1|}, \tag{81}$$

dependent on the incident angle θ.

Next we set up a curved boundary, with the curvature radius $R_{\rm S}$, as shown in Fig. 4(b). Here we focus on the behavior at a long wavelength so that the uncertainty in the position can be neglected. Introducing an incident plane wave with the wave number k in the x-direction, its incident angle θ on the boundary depends on the lateral incident position y, as $\theta(y) = \arcsin(y/R_{\rm S})$, leading to the phase factor $e^{i\gamma(\theta(y))}$ for the scattered wave. The phase $\gamma(\theta)$ defined by Eq. (81) can be expanded around $\theta = 0$ as

$$\gamma(\theta) = \pi + \mu\theta + O(\theta^2) = \pi + \tilde{k}y + O(y^2), \tag{82}$$

where $\tilde{k} = \mu/R_{\rm S}$. Noting the inequality

$$\cos\zeta(1-\sin\zeta)^{-1} > \cos\zeta, \tag{83}$$

the factors μ and $\tilde{k}$ here are negative. Therefore, the phase factor can be approximated as

$$e^{i\gamma(\theta)} = -e^{i\tilde{k}y+O(y^2)}, \tag{84}$$

which can be interpreted as the transverse wave component, accounting for the scattering skewness. Since the phase $\gamma(\theta)$ takes the opposite sign if the sign of $n_z(\boldsymbol{r})$ is flipped, the scattering skewness is sensitive to the skyrmion number.